JOURNAL OF APPLIED ELECTROCHEMISTRY 26 (1996) 843–852

# Nucleation and crystal growth in gold electrodeposition from acid solution Part I: Soft gold

Y. G. LI, W. CHRZANOWSKI*, A. LASIA

*Département de Chimie, Université de Sherbrooke, Sherbrooke, Québec, J1K 2R1, Canada*

Received 14 August 1995; revised 25 January 1996

The initial stages of gold electrodeposition on a gold electrode were studied in a proprietary bath (Renovel N) using linear sweep voltammetry and chronoamperometry. Tafel plots with two different slopes were obtained, indicating that the mechanism for gold deposition depends on potential. An inhibition phenomenon was observed during gold electrocrystallization. Experimental current–time transients were analysed using nonlinear least-squares approximations by various models of nucleation and crystal growth. The electrodeposition mechanism changes from three-dimensional progressive at lower overpotentials to three-dimensional instantaneous at higher overpotentials. Moreover, additional two-dimensional progressive or a secondary three-dimensional progressive processes take place in certain potential ranges. It was shown that the outward growth rate of the substrate's base plane displays a linear Tafel relationship whereas the vertical growth rate of gold crystals decreases at more negative potentials due to an inhibition process.

## 1. Introduction

Gold is extensively used in the electronic industry due to its good electrical conductivity and high corrosion resistance [1, 2]. The industrial significance of gold deposits has resulted in various, usually proprietary, plating formulations. Among them, a citrate-based acid solution with less toxicity in comparison with alkaline cyanide solutions, became frequently used for gold plating, especially for hard gold plating. Numerous studies [3–28] have been undertaken on the reaction kinetics, physical properties and structural aspects of gold deposit from both proprietary and non-proprietary solutions. Most recently, Bocking and coworkers [29, 30] have studied the structures of gold and gold alloys from various proprietary electrolytes.

The kinetics of nucleation and crystal growth in the initial stages of deposition, which depends on the solution composition, pH, temperature, nature of substrate etc., influence the physical properties and the morphology of deposits. Unlike systems such as nickel and zinc, whose mechanisms of nucleation and crystal growth have been widely studied, relatively little information is available on gold. Only one publication dealt with the nucleation and crystal growth during gold deposition from a citric acid solution from a morphological point of view [28]. There are no publications dealing with the kinetics of nucleation and crystal growth of gold deposited in acid solutions.

The aim of the present paper is to investigate the mechanism of nucleation and growth during gold deposition from a commercial proprietary citrate acid solution (Renovel N bath, Lea Ronal). It should be mentioned that this proprietary electrolyte was also used by Bocking and coworkers [29, 30] in the structural studies of gold deposits. In our previous paper [31] linear sweep voltammetry and Tafel plots were discussed. In the present paper detailed chronoamperometric studies were carried out in a wide potential range for soft (pure) gold deposition. Information on the kinetics of gold electrocrystallization was obtained from the analysis of current–time transients. In Part II [32], studies of nickel hardened gold deposition are presented.

## 2. Theory of nucleation and crystal growth

Theory of nucleation and crystal growth phenomena has been reviewed in the literature [33, 34]. It was shown that a chronoamperometric method is a powerful tool for studying the nucleation and crystal growth mechanism during the initial stages of metal electrocrystallization.

Once nucleation begins, crystals growth may be determined by the rate of charge-transfer or diffusion processes. In a simple case of charge-transfer control under potentiostatic condition, equations describing two- or three-dimensional nucleation and crystal growth processes occurring on a foreign substrate are well known [33, 34]. For two-dimensional (2D) instantaneous nucleation and cylindrical growth current is described as [33, 34]

$$i = \frac{2zF\pi hMN_0k_{2D}^2t}{\rho}\exp\left(-\frac{\pi M^2N_0k_{2D}^2t^2}{\rho^2}\right) \quad (1)$$

* On leave from the Technical University of Gdansk, 80-952 Poland.

0021-891X 

and for 2D progressive nucleation

$$i = \frac{zF\pi hMk_{2D}^2 A_{2D} t^2}{\rho} \exp\left(-\frac{\pi M^2 k_{2D}^2 A_{2D} t^3}{3\rho^2}\right) \quad (2)$$

where $k_{2D}$ is the lateral growth rate constants (mol $cm^{-2} s^{-1}$), $h$ the layer height (cm), $N_0$ the total number of active centres ($cm^{-2}$), $A_{2D}$ the nucleation rate (nuclei $cm^{-2} s^{-1}$), $M$ the atomic weight ($g mol^{-1}$) and $\rho$ the density ($g cm^{-3}$) of the deposit. For these mechanisms the observed current initially increases and then decreases to zero when the surface is completely covered by the two-dimensional crystals. For three dimensional (3D) instantaneous nucleation and growth of right-circular cones, current is given by [33, 34]:

$$i = zFk'\left[1 - \exp\left(-\frac{\pi M^2 k^2 N_0 t^2}{\rho^2}\right)\right] \quad (3)$$

and for 3D progressive nucleation:

$$i = zFk'\left[1 - \exp\left(-\frac{\pi M^2 k^2 A_{3D} t^3}{3\rho^2}\right)\right] \quad (4)$$

where $k$ and $k'$ are, respectively, the lateral and vertical growth rate constants (mol $cm^{-2} s^{-1}$) and $A_{3D}$ the nucleation rate (nuclei $cm^{-2} s^{-1}$). Equations 3 and 4 predict that the observed current increases and then reaches a plateau at longer times.

When nucleation and growth processes occur on the same substrate, the transient current for crystal growth is similar to those on foreign substrates, except that the outward growth on the same substrate's base plane has to be taken into account. This model was developed by Harrison and Thirsk [34]. The observed current in the case of 3D nucleation consists of two parts: namely, current due to three-dimensional crystal growth, $i_{3D}$, and the current due to outward growth on a substrate base plane at a free surface uncovered by growing nuclei, $i_f$. The total current, for instantaneous nucleation, is given as

$$i = i_f + i_{3D} = zFk_0 \exp\left(-\frac{\pi M^2 k^2 N_0 t^2}{\rho^2}\right) + zFk'\left[1 - \exp\left(-\frac{\pi M^2 k^2 N_0 t^2}{\rho^2}\right)\right] \quad (5)$$

and for progressive nucleation

$$i = i_f + i_{3D} = zFk_0 \exp\left(-\frac{\pi M^2 k^2 A_{3D} t^3}{3\rho^2}\right) + zFk'\left[1 - \exp\left(-\frac{\pi M^2 k^2 A_{3D} t^3}{3\rho^2}\right)\right] \quad (6)$$

where $k_0$ is the growth rate constant on the base plane of the substrate.

Equations 5 and 6 predict formation of a current minimum at beginning and a current plateau at longer times. A model similar to Equation 5 has been used to interpret the nucleation and growth phenomena during electrocrystallization of Au [21], Cu [35] and Pd [36] on the same substrate.

Nucleation and growth phenomena are affected by many factors and sometimes different processes may occur simultaneously: that is, a combination of 2D and 3D growth [37, 38], the death and rebirth of nuclei [38], the secondary 3D growth on top of the first growth layers [39] etc.

## 3. Experimental details

### 3.1. *Composition of solutions*

A commercial proprietary bath based on a Renovel N make-up solution (Lea Ronal), was used for gold-plating. It contains citrate-based electrolyte and a current extender (principally nicotinamide) [29, 30]. Two different solutions, A and C, were studied. Solution A was prepared by mixing 75% (by volume) of the proprietary supporting electrolyte (Renovel N) with 25% of deionized water. Solution C used for the soft gold deposit was prepared by mixing aqueous gold cyanide $KAu(CN)_2$ (SEL–REX, Enthone–OMI) solution (25%) with the Renovel make-up solution (75%). The concentration of gold in solution C was 0.091 M. Deionized water (Barnstead, Nanopure) was used in all experiments. pH of solutions was adjusted with KOH to 4.4. All other reagents and chemicals used were of analytical grade.

### 3.2. *Electrochemical procedures*

A three-compartment electrochemical cell with cathodic compartment of ~250 ml was used and anodic compartment was separated by Nafion® 117 (DuPont) membrane in all measurements. The cathodic compartment was thermostated at 60 ± 0.5 °C. The anodic part was always filled with solution A. A gold rotating disc electrode (RDE) (area 0.0707 $cm^2$) was used as a working electrode. The rotation rate of the RDE was controlled by the AFASR rotator (Pine). Prior to each measurement, the working electrode was polished on a rotating table (GP-60 Polisher, Leco Corp.) with 1 μm and 0.05 μm alumina powder (Gamma Micropolish Alumina, Buehler), washed thoroughly with water, degreased with methanol, kept in a concentrated $HNO_3$ for 10 s, and again rinsed thoroughly with water. The reference electrode was a saturated calomel (SCE), it was connected to the cell via a bridge equipped with a Luggin capillary probe and filled with the studied solution. All the potentials were referred to this electrode. A platinum mesh was used as a counter electrode. Solution in the cathodic compartment was deoxygenated with oxygen-free nitrogen for at least two hours prior to each run and during the measurement nitrogen was passed over the solution. The potentiostat/galvanostat (model 263, EG&G PAR) was controlled by a PC microcomputer using PAR M270/250 program. *IR* compensation was utilized to eliminate solution resistance. The latter was determined by a.c. impedance method. In

chronoamperometric measurements, potential steps were applied from 0 V (vs SCE), in which no gold deposition occurs, to a potential $\leqslant -0.5$ V at which the deposition starts.

## 4. Results

### 4.1. *Linear sweep voltammetric measurements*

Linear sweep voltammetric (LSV) measurements are described elsewhere [31]. Figure 1 curve (a) shows a voltammogram of a supporting electrolyte (solution A) on Au RDE. A small current was recorded at potentials more positive than −0.725 V. It was probably caused by the reduction of traces of oxygen in the solution. The current increased abruptly as potential became more negative than −0.725 V due to the hydrogen evolution reaction (HER). Hydrogen gas bubbles on the surface were observed at about −1.2 V. Theoretically, the equilibrium potential for HER in this solution is about −0.5 V, however, higher overpotentials are needed for the HER to appear on gold electrode. This reaction could influence the mechanism of gold deposition, especially in the initial stages of nucleation and crystal growth. Furthermore, it was found that LSVs of blank solution were not reproducible when the measurements were repeated without any pretreatment of the electrode. A slightly darkened solid film was observed on the surface of the gold electrode after about 10 cycles. This film was insoluble in water but could be removed with a Kimwipe. The reduction of which compound contributed to the film formation is not yet known.

The LSV measurement of gold deposition on Au RDE is also shown in Fig. 1 (curve (b)). These measurements in solution C were reproducible even without pretreatment of the electrode. The current started to increase at a potential of about −0.35 V, indicating the onset of gold deposition. Two potential regions were clearly seen. At more positive potentials, a current peak appeared on the LSVs; in other words, the current initially increased with potential, formed a maximum and then decreased forming a minimum. In a second potential range, the current increased abruptly as the potential became more negative,

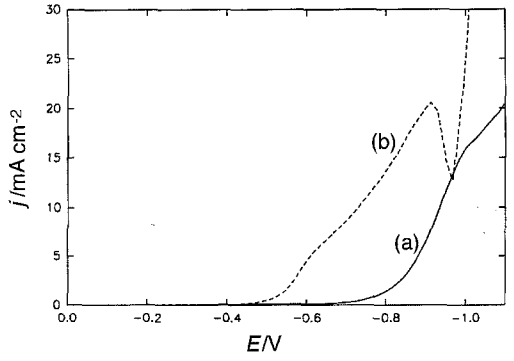


Fig. 1. Linear sweep voltammograms obtained on Au rotating disc electrode in solution A (curve (a)) and C (curve (b)), sweep rate 1 mV $s^{-1}$, rotation speed 650 rpm.

which corresponds to the gold deposition simultaneously with the hydrogen evolution.

We have already shown [31] that current peaks on LSV increase with the rotation rate. An obvious current peak was observed even under high rotation speed of 4000 rpm. Furthermore, this peak decreased with the increase in the sweep rate. These observations, together with the fact that the peak current was much lower than the diffusion limited one, predicted by Levich equation for $Au(CN)_2^-$ reduction, indicate that this process is under kinetic control [31]. As mentioned above, the HER in acid solutions becomes important at very negative potentials. Roev and Gudin [40] found that the HER can result in the formation of a peak on LSVs before the bulk deposition of Zn–Ni alloy. To determine whether the LSV peak observed during gold deposition is related to the HER, LSV measurements were performed in solutions of different pH. If the HER contributes significantly to this process the peak height should be larger at lower pH (higher concentration of $H^+$) [40]. However, it was found that peak height increases with pH (not shown): for example, peak current density increases about 10% as pH of bath increases from 4.4 to 5.1. Therefore, this result allows us to conclude that the peak observed on LSVs is neither associated with the diffusion process of gold cyanide species nor with the HER, and it is most probably caused by an inhibition process.

### 4.2. *Chronoamperometric measurements*

To decrease the influence of mass transfer on the deposition process, all chronoamperometric measurements were performed at the rotation speed of 4000 rpm. Figure 2 illustrates a set of current–time transients in a wide potential range obtained in solution C. The initial current decrease could be, in general, caused by four different processes: (i) a double layer charging current, which decreases exponentially to zero in microseconds; (ii) a transient diffusion limited process. For diffusion controlled processes on a rotating disc electrode, the current should decrease to a steady-state value after certain time of potential imposed on RDE. The time necessary to reach a steady state, depends on the rotation rate. Under the conditions used, this time was estimated as about 0.03 s at a rotation speed of 4000 rpm [41]; (iii) a direct deposition of metal into lattice without nucleation; and (iv) other side reactions, such as hydrogen evolution, whose influence becomes obvious only at very negative potential.

The current minimum, $i_{min}$, observed at beginning of current transients increases with negative potential. The time, $t_{min}$ corresponding to current minimum extends to a few seconds, depending on the potential applied, and the charge consumed up to $t_{min}$ corresponds to more than ten compact gold monolayers ($\sim 204\ \mu C\ cm^{-2}$ per monolayer) which suggests that gold deposition process starts before $t_{min}$ is reached. The initial current minimum corresponds principally

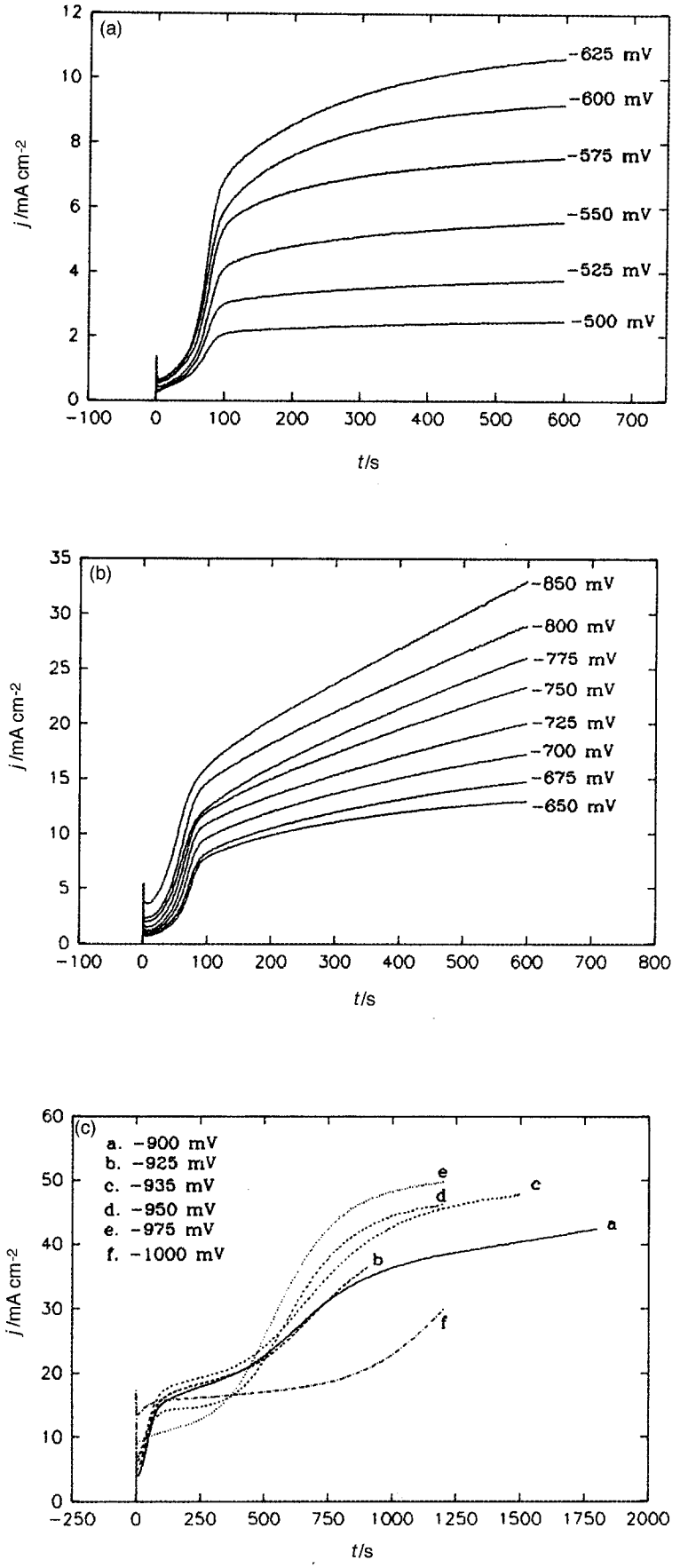


Fig. 2. Experimental current–time transients for soft gold deposition on Au RDE from solution C, rotation speed 4000 rpm.

to a direct gold deposition without nucleation. After an induction time, the nucleation process starts and gold crystals grow. This leads to an increase of current with time as result of the increase of the electroactive surface area. The shape of the current–time transients is determined by the nucleation and crystal growth processes, which depend strongly on the potential applied. At potentials between −0.500 V and −0.850 V, the current first increases quickly and then continues to increase slowly over longer times. In this potential range, no steady state is reached, not even after a relatively long time. A slow increase of current over longer times may be related to a second growth process occurring on the top of the initially deposited layers. Furthermore, it was noticed that at low overpotentials (e.g., −0.50 V) the increase of current with time at the foot of transients was quite slow. This may imply that two different nucleation and growth processes occur simultaneously.

When potential is more negative than −0.90 V, Fig. 2(c), the current increases rapidly with time and then reaches a quasi-plateau. Later, current continues to increase slowly with time and another plateau is observed at longer times. This implies a second three-dimensional nucleation and growth process on the top of the initial deposit. The current of the second plateau increases with negative potentials in the range −0.90 to −0.975 V. The first quasi-plateau increases as potential changes from −0.90 to −0.935 V, and then decreases with negative potential in the range −0.95 to −0.975 V. This may be caused by an inhibition process, that is, crystal growth is inhibited by a certain substance produced on the electrode surface. This is consistent with the conclusions from the LSV measurements. At potentials more negative than −1.0 V (corresponding to a second potential range on LSVs), the induction time for nucleation becomes very short, the current increases and reaches a small plateau faster. At later stages, the current continues to increase and no steady state is observed; in other words, the current increases with negative potential. The HER becomes important at potentials more negative than −1.0 V.

Deposits exhibit different appearances at different potentials. Bright smooth deposits were observed at potentials more positive than the peak potential on LSVs. The surface changed from bright to dull as potentials became more negative than the peak potential. Thereafter, in the second potential region, deposits were usually bright and smooth. We have performed the morphological studies of gold deposits on copper substrate using scanning electron microscopy (SEM) and atomic force microscopy (AFM). It was shown that the growth morphology is strongly potential-dependent and grains with various sizes are observed. These results will be presented in a further paper [42].

Since no steady-state for gold deposition was reached under most experimental conditions, the current over longer times could not be used to construct Tafel plots. A Tafel plot based on the initial current

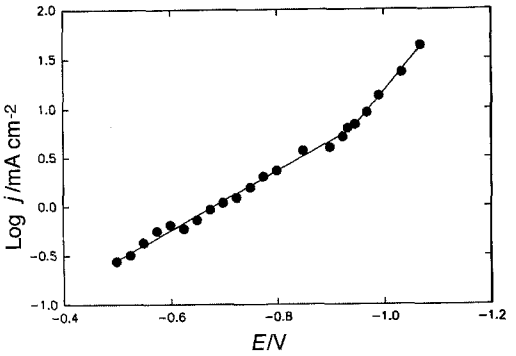


Fig. 3. Tafel plot constructed on the basis of the initial current minimum shown in Fig. 2, for soft gold deposition from solution C.

minima is shown in Fig. 3. Two linear regions with two different slopes are observed. Tafel slopes are $0.328 \pm 0.007\,\mathrm{V\,dec^{-1}}$ in potential range from −0.50 to −0.95 V and $0.157 \pm 0.006\,\mathrm{V\,dec^{-1}}$ at potentials between −0.95 to −1.1 V, respectively. These values are in a good agreement with the results obtained from the chronopotentiometric measurement, for which Tafel plots were based on the initial potential peak on the potential–time transients [31].

## 5. Analysis of experimental results and discussions

### 5.1. *Mechanism of gold deposition*

It is generally accepted that gold deposition proceeds via two different mechanisms at different overpotentials ranges [11–14]. At lower overpotentials, it occurs via an adsorption of AuCN followed by the electron-transfer, that is,

$$Au(CN)_2^- + H^+ \rightleftharpoons AuCN_{ads} + HCN \qquad (7)$$

and

$$AuCN_{ads} + H^+ + e^- \rightarrow Au + HCN \qquad (8)$$

To a certain extent, deposition of gold on the electrode covered by $AuCN_{ads}$ might be similar to the deposition on a foreign substrate, nucleation is needed to initiate the deposition process. In the case of specific adsorption of charged intermediates, the actual charge transfer occurs across a fraction of the Helmholtz layer only, leading to the deviation of the charge transfer coefficient from 0.5 [43]. Hence, the Tafel slope is expected to be relatively high [14].

At higher overpotentials, gold deposition occurs via direct charge-transfer reaction as:

$$Au(CN)_2^- + 2H^+ + e^- \rightarrow Au + 2HCN \qquad (9)$$

Tafel slope in this region would be expected to be lower. At intermediate overpotentials, the competition between reduction of AuCN and $Au(CN)_2^-$ from solution may take place.

Adsorbed AuCN is an intermediate on the surface of a growing film in the electrocrystallization of gold from cyanide solutions [44, 45]. Moreover, so-called polymers are also codeposited into bulk gold [46–48]. Undoubtedly, adsorption of AuCN and the incorpora-

tion of impurities into gold deposits have an important effect on the nucleation and growth mechanism.

In acidic solutions, two important factors should be considered. First, the mechanism of gold deposition may be modified by the HER. Moreover, concentration of free cyanide ions, $CN^-$, is initially very low due to high acidity of the bath. Hence, generation of cyanides during deposition may play an important role on gold deposition from acidic solutions. Since the equilibrium of the chemical adsorption, Reaction 7, may be shifted to the left by production of $CN^-$ or HCN adsorbed on the surface, this way result in a self-inhibition effect on Reactions 7 and 8. Note that $Au(CN)_2^-$ is electroactive only at higher overpotentials, Reaction 9, and the production of HCN or $CN^-$ has a less influence on Reaction 9 than Reaction 8.

It was found earlier [31] that on using a bath which had not been used for some time a smooth gold deposit may only be obtained after passing some charge to reduce the gold. This reduction increases amount of HCN in the solution. It is known that cyanides may be adsorbed on the surface of the gold electrode at the negative potential region [49, 50]. However, because the concentration of cyanides in alkaline solution is relatively high, the effect of $CN^-$ generated during the gold deposition in Reaction 7 may be ignored. Although the reduction prewave for $AuCN_{ads}$ on voltammograms in alkaline solutions was observed [7, 8, 10, 11, 14], the behaviour described earlier is different from that observed in our case. It was claimed [10, 14] that the height of the prewave for $AuCN_{ads}$ was independent of rotation speed. This is in contradiction with our observation [31]. It is possible that the adsorption of AuCN is not influenced by the $CN^-$ mass transfer when their concentration is high enough (alkaline cyanide baths). During gold deposition from acid solution the mass transfer of HCN from the surface into bulk of solution is probably under diffusion control. The height of the prewave corresponding to $AuCN_{ads}$ in alkaline solutions is much lower [7, 8, 11] than the peak height of LSVs recorded under our conditions. This may imply that an inhibition caused by the $CN^-$ species for gold deposition in alkaline solutions is stronger, due to the higher concentration of $CN^-$ in these solutions.

Adsorption of AuCN might also be affected by other factors, for example, the composition of solution, pH, applied potential and the nature of the substrate. A competitive adsorption of additives may also occur and this would influence the adsorption of AuCN and $CN^-$ or HCN.

### 5.2. *Approximations of current–time transients: nucleation and crystal growth models*

Information about the nucleation and crystal growth may be obtained from analysis of the current–time transients in initial stages of electrocrystallization. As shown in Fig. 2, the shapes of these transients

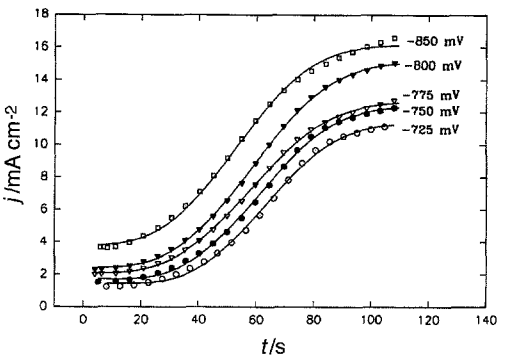


Fig. 4. Initial portions of current-time transients shown in Fig. 2 at potentials from −0.725 to −0.850 V. Points: experimental; solid lines: theoretical fit to Equation 10.

are different at different potentials. This indicates that the nucleation and growth mechanism depends strongly on the potential applied. To approximate initial portions of the experimental current–time transients, various 2D and 3D models were tested.

Assuming that 3D progressive nucleation and growth of right-circular cones occurs onto the same substrate, the current consists of two parts as indicated in Equation 6: the first term decreases to zero with time, while the second term reaches a plateau. We may express this as

$$i = i_0 \exp(-P_2 t^3) + P_1[1 - \exp(-P_2 t^3)] \qquad (10)$$

where $i_0 = zFk_0$; $P_2 = \pi M^2 k^2 A_{3D}/3\rho^2$ and $P_1 = zFk'$, other symbols have been explained earlier. Figure 4 shows current–time transients fitted to Equation 10 in the potential range from −0.725 to −0.85 V. However, transients recorded at more positive potentials could not be described well by this model, especially at the foot of the curves, where current increases rather slowly with time. It is possible that there is also another process whose contribution decreases with negative potentials. To describe the current–time transients recorded at potentials between −0.5 V and −0.725 V, it was supposed that a 2D progressive nucleation and crystal growth of cylinders, Equation 2, occurs simultaneously with the main process of 3D progressive nucleation and growth of right-circular cones. Therefore, the total current consists of three parts:

$$i = i_f + i_{2D} + i_{3D} \qquad (11)$$

where a 3D growth process occurs after the induction time $t_0$. The total current is given by

$$i = i_0 \exp(-P_4 t^3) + P_3 t^2 \exp(-P_4 t^3) + P_1[1 - \exp(-P_2 (t - t_0)^3)] \qquad (12)$$

where $i_0 = zFk_0$, $P_1 = zFk'$, $P_2 = \pi M^2 k^2 A_{3D}/3\rho^2$, $P_3 = zF\pi hMk_{2D}^2 A_{2D}/\rho$ and $P_4 = \pi M^2 k_{2D}^2 A_{2D}/3\rho^2$.

Figure 5 shows the theoretical fit to the experiment data using Equation 12. The fit is very good. Contributions of two growth processes, at potential −0.500 V and −0.725 V, are illustrated in Fig. 6. The contribution of the 2D process (curves (a′) and (b′)) decreases as potential becomes more negative and it is negligible at high negative potentials.

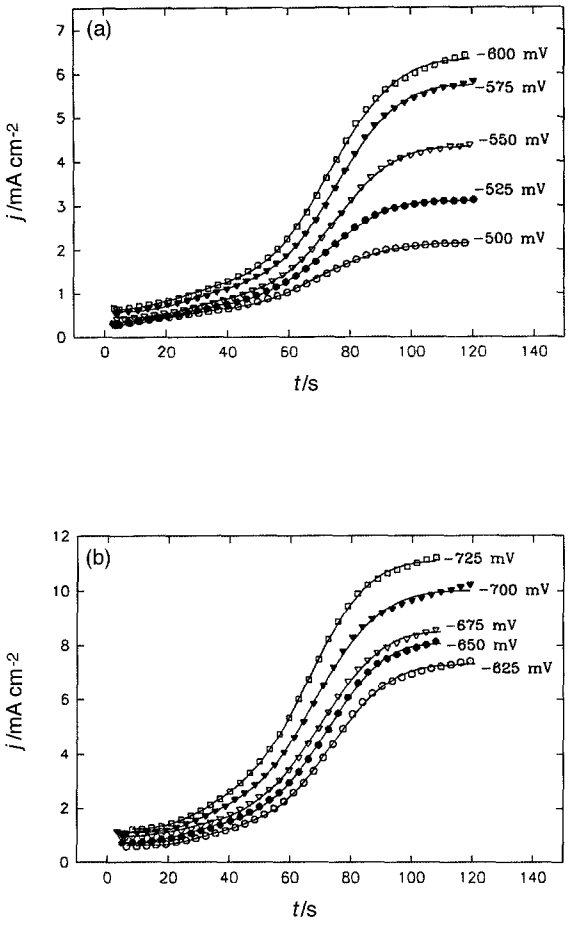


Fig. 5. Initial portion of current–time transients shown in Fig. 2 at potentials from −0.500 to −0.725 V. Points: experimental; solid lines: theoretical fit to Equation 12.

When the potential is more negative than −0.90 V, two quasi-plateaux appear on the current–time transients, as shown in Fig. 2(c). In modelling of the complete transients it was assumed that a secondary 3D progressive nucleation and growth process occurs on the top of first one after a certain induction time. The first growth process becomes 3D instantaneous

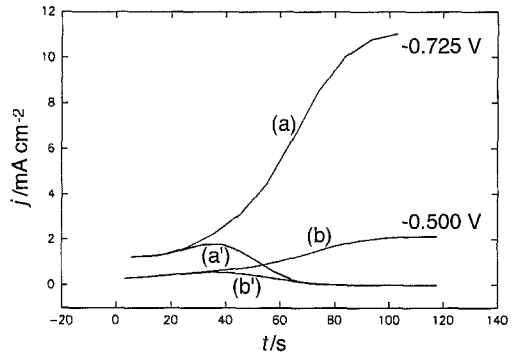


Fig. 6. Simulated current–time transients according to Equation 12 at −0.500 V (curves (b) and (b′) and −0.725 V (curves (a) and (a′)), total current (curves (a) and (b)), and the contribution of a 2D growth process (curves (a′) and (b′)). The parameters used were determined experimentally; curves (b) and (b′) ($E = -0.500$ V): $i_0 = 0.303 \pm 0.003$ mA cm$^{-2}$, $P_1 = 2.139 \pm 0.004$ mA cm$^{-2}$, $t_s = 20.5 \pm 2.9$ s, $P_2 = (7.37 \pm 0.92) \times 10^{-6}$ s$^{-3}$, $P_3 = (4.25 \pm 0.12) \times 10^{-4}$ mA cm$^{-2}$ s$^{-2}$, $P_4 = (9.16 \pm 0.01) \times 10^{-5}$ s$^{-3}$; curves (a) and (a′) ($E = -0.725$ V): $i_0 = 1.238 \pm 0.020$ mA cm$^{-2}$, $P_1 = 11.11 \pm 0.02$ mA cm$^{-2}$, $t_s = 18.7 \pm 1.3$ s, $P_2 = (2.088 \pm 0.057) \times 10^{-6}$ s$^{-3}$, $P_3 = (2.11 \pm 0.10) \times 10^{-3}$ mA cm$^{-2}$ s$^{-2}$, $P_4 = (2.19 \pm 0.23) \times 10^{-5}$ s$^{-3}$.

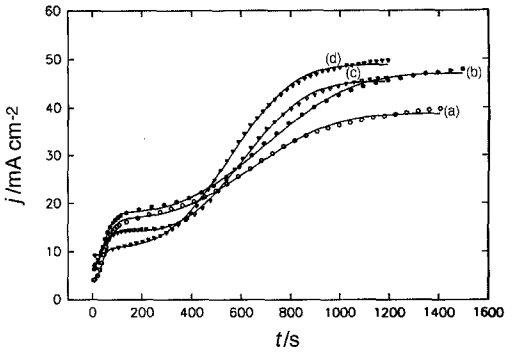


Fig. 7. Current–time transients for soft gold deposition from solution C at potentials between −0.900 V and −0.975 V. Points: experiment; solid line: theoretical fit to Equations 13 and 14. Derived parameters: (a) $E = -0.900$ V: $i_0 = 4.53 \pm 0.16$ mA cm$^{-2}$, $P_1 = 16.84 \pm 0.35$ mA cm$^{-2}$, $P_2 = (2.84 \pm 0.12) \times 10^{-4}$ s$^{-2}$, $P_s = 21.97 \pm 0.15$ mA cm$^{-2}$, $P_{2s} = (2.58 \pm 0.06) \times 10^{-9}$ s$^{-3}$, $t_s = 100.5 \pm 6.5$ s; (b) $E = -0.935$ V: $i_0 = 6.37 \pm 0.20$ mA cm$^{-2}$, $P_1 = 18.05 \pm 0.41$ mA cm$^{-2}$, $P_2 = (2.91 \pm 0.14) \times 10^{-5}$ s$^{-2}$, $P_s = 29.05 \pm 0.22$ mA cm$^{-2}$, $P_{2s} = (2.10 \pm 0.12) \times 10^{-9}$ s$^{-3}$, $t_s = 14.1 \pm 1.5$ s. (c) $E = -0.950$ V: $i_0 = 7.03 \pm 0.15$ mA cm$^{-2}$, $P_1 = 14.24 \pm 0.32$ mA cm$^{-2}$, $P_2 = (3.83 \pm 0.28) \times 10^{-4}$ s$^{-2}$, $P_s = 31.23 \pm 0.15$ mA cm$^{-2}$, $P_{2s} = (5.78 \pm 0.22) \times 10^{-9}$ s$^{-3}$, $t_s = 125.7 \pm 6.3$ s. (d) $E = -0.975$ V: $i_0 = 9.16 \pm 0.21$ mA cm$^{-2}$, $P_1 = 10.04 \pm 0.14$ mA cm$^{-2}$, $P_2 = (3.49 \pm 0.12) \times 10^{-4}$ s$^{-2}$, $P_s = 37.89 \pm 0.18$ mA cm$^{-2}$, $P_{2s} = (5.19 \pm 0.17) \times 10^{-9}$ s$^{-3}$, $t_s = 47.8 \pm 6.1$ s.

nucleation and growth of right circular cones. The observed current is described as

$$i = i_0 \exp(-P_2 t^2) + P_1[1 - \exp(-P_2 t^2)] \qquad (13)$$

for $t \leqslant t_s$ and

$$i = i_0 \exp(-P_2 t^2) + P_1[1 - \exp(-P_2 t^2)] + P_s[1 - \exp(-P_{2s}(t - t_s)^3)] \qquad (14)$$

for $t \geqslant t_s$ where $P_2 = \pi M^2 k^2 N_0/\rho^2$, $P_s = zFk'_s$, $P_{2s} = \pi M^2 k_s^2 A_s/3\rho^2$, $k'_s$ and $k_s$ are the vertical and lateral growth rate constants for secondary growth process, respectively; $A_s$ is the nucleation rate for the secondary nucleation process and $t_s$ its induction time. Figure 7 presents experiment data and the fitted curves according to Equations 13 and 14 at potentials between −0.9 and −0.975 V. It is obvious that the observed current transients may be well described by the proposed model.

From the analysis presented above, kinetic parameters were estimated. Figure 8 shows a Tafel plot of the outward growth rate constant, $k_0$, for the substrate's base plane. The dependence of the vertical

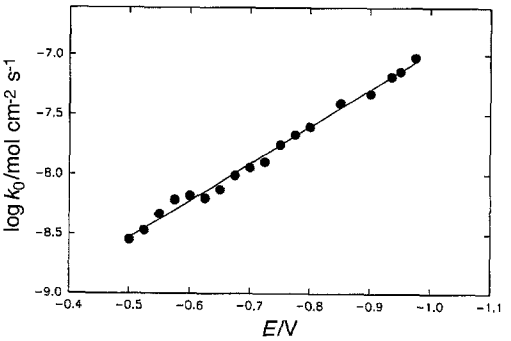


Fig. 8. Plot of the logarithm of outward growth rate constant for substrate base plane, $\log k_0$, against potential for soft gold deposition from solution C.

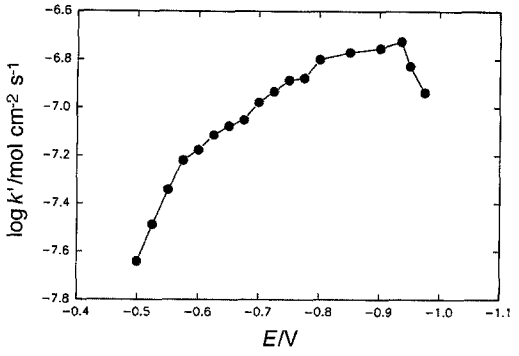


Fig. 9. Plot of the logarithm of vertical growth rate constant, $\log k'$, against potential for soft gold deposition from solution C.

growth rate constant, $k'$, on the potential for the first 3D growth process is shown in Fig. 9. A nonlinear dependence of $\log k'$ against potential was found. The rate constant $k'$ increases as potential becomes more negative from −0.500 to −0.935 V and then decreases as potential changes from −0.935 to −0.975 V, indicating that crystal growth in the direction perpendicular to the substrate surface is inhibited, probably due to a self-inhibition process caused by cyanide species [31]. The self-inhibition effect on crystal growth in gold deposition from phosphate electrolyte was also observed by Davidovic and Adzic [22]. They suggested the adsorption of cyanide species or other impurities is the reason of such an effect. However, the vertical growth rate, $k'_s$, for the secondary growth process at potentials −0.90 to −0.975 V increases linearly with negative potential (Fig. 10), similar behaviour was also reported in zinc deposition [39]. The dependence of the combined rate constant, $k^2A_{3D}$, for the lateral growth of the first 3D growth process is shown in Fig. 11. Although the obtained points are somewhat scattered, it seems that potential applied does not have a big influence on this parameter. Supposing that the growth rates in two different directions are the same, the nucleation rate, $A_{3D}$, may be estimated. It decreases as potential becomes more negative, as shown in Fig. 12. This is in contrast to a classical thermodynamic and an atomistic nucleation theories [51]. Although the classical theory applies to large clusters only, and the atomistic theory to small ones, both predict an increase of the nucleation rate with the increase in overpotential. The obtained results imply that nucleation of gold in our experiments is

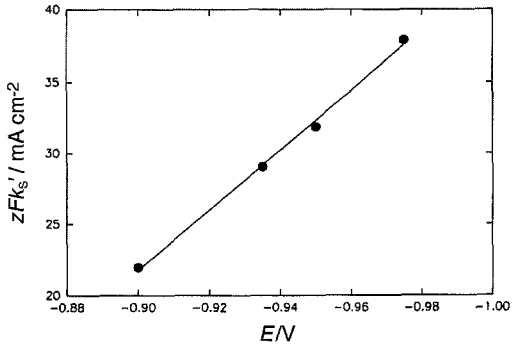


Fig. 10. Plot of current for a secondary growth process, $zFk_s$, determined from Equation 14, against potential in the range from −0.900 to −0.975 V.

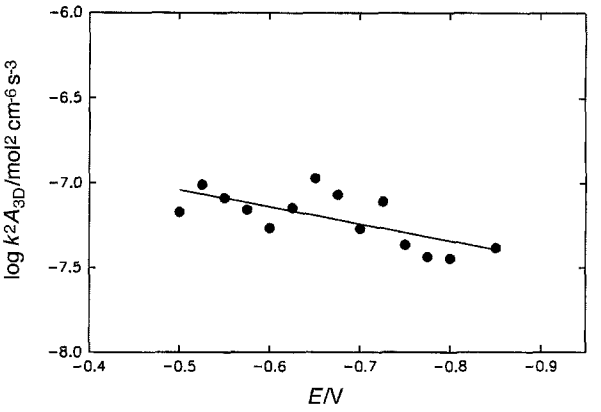


Fig. 11. Plot of $\log k^2A_{3D}$, determined from Equations 10 and 12, against potential for soft gold deposition from solution C.

inhibited, probably because active sites for nucleation are partially blocked by adsorbates. At potentials −0.9 to −0.975 V, the total number of nuclei for instantaneous nucleation for first growth process is estimated to be $2.5 \times 10^7$ to $9.6 \times 10^7$ nuclei $cm^{-2}$, only slightly increasing with negative potential.

Generally, during metal deposition without inhibition, the dependence of both the initial minimum and the plateau current (recorded at longer times in chronoamperometric curves) against potential displays tafelian behaviour [21, 35, 36]. In our case, only the dependence of the initial minimum current density shows such behaviour, indicating that the growth of substrate's base plane is not inhibited probably because at this time the concentration of cyanides generated on electrode surface is very low and their inhibition effect may be neglected. However, dependence of the plateau current density against potential does not show a simple tafelian behaviour. The surface concentration of cyanides is higher at longer times and the vertical growth of 3D centres is thus retarded.

In the above analysis nucleation and crystal growth mechanism varied with the applied potential. Similar procedures were used by Creus *et al.* [37] and Abyaneh *et al.* [38, 39] for various nucleation and crystal growth processes occurring simultaneously. It should be added that other 2D and 3D processes were also tried but the models presented above gave the best and

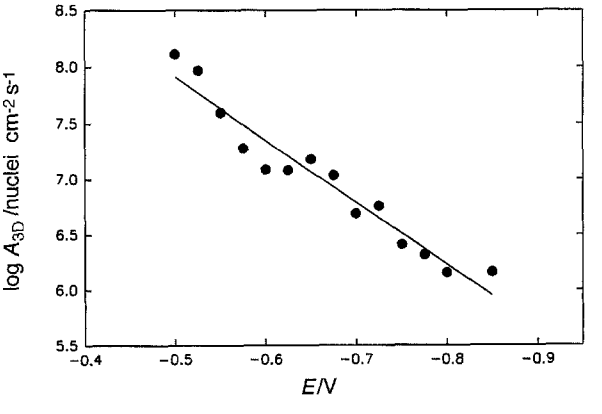


Fig. 12. Plot of nucleation rate of soft gold in solution C, $A_{3D}$, Equations 10 and 12, against potential assuming that the growth rate constants in vertical and lateral directions are equal.

statistically distinguished results. The current–time transients recorded at potentials more negative than −1.0 V could not be analyzed and they were largely influenced by the HER.

## 6. Conclusions

The results presented above show that gold deposition from Renovel N bath proceeds via two different mechanisms. At the more positive potentials in the range from −0.50 V to −0.95 V, a higher Tafel slope of 0.328 V dec$^{-1}$ was obtained, indicating that deposition reaction occurs via adsorption of AuCN followed by the charge-transfer step. At more negative potentials, a lower Tafel slope of 0.157 V dec$^{-1}$ was obtained, corresponding to the mechanism of a direct charge-transfer together with the HER.

It was concluded from linear sweep voltammetric measurement that the inhibition phenomena occur during gold deposition at more positive potentials. This conclusion was further confirmed by the analysis of experimental current–time transients.

The mechanisms of nucleation and crystal growth in the initial stages of gold electrocrystallization depends strongly on potentials applied. The 2D progressive nucleation and crystal growth of cylinders, and the 3D progressive nucleation and growth of right circular cones occur simultaneously at lower overpotentials. The contribution of the 2D process decreases with negative potential and then becomes negligible. At potentials between −0.725 and −0.85 V, a simple model of 3D progressive nucleation and crystal growth of right-circular cones well describes the initial portion of experimental curves. Nucleation changes from progressive at potentials between −0.725 and −0.85 V to instantaneous at more negative potentials between −0.90 V and −0.975 V. A secondary 3D progressive nucleation and growth process was found to occur on the top of the first layers at potentials from −0.90 to −0.975 V. Kinetic parameters $k_0$, $k'$, $k$, $N_0$ and $A_{3D}$ were estimated. It was shown that vertical growth of crystals is inhibited by a poison produced on the surface. The dependence of the vertical growth rate constant on potential applied showed a nonlinear dependence on potential due to the inhibition process. Nucleation rate of gold deposition decreases with negative potential, in contrast to the nucleation theories, implying that nucleation process is also inhibited.

The dependence of growth rate for the substrate's base plane on potential applied shows a linear tafelian dependence. The initial minima on the current–time transients correspond to the outward growth of substrate's base plane and may be used to construct Tafel plots in the case of metal electrocrystallization onto the same substrate.

## Acknowledgements

Financial support from the NSERC is gratefully acknowledged.

## References

[1] I. R. Christie and B. P. Cameron, *Gold Bull.* **27** (1994) 12.
[2] F. R. Schlodder, H. H. Beyer and W. G. Zilske, 'GOLD 100': Proceedings of the International Conference on Gold, Johannesburg (1986), vol. 3, p. 21.
[3] H. Y. Cheh, *J. Electrochem. Soc.* **118** (1971) 551.
[4] H. G. Silver, *ibid.* **116** (1969) 26C.
[5] H. Angerer and N. Ibl, *J. Appl. Electrochem.* **9** (1979) 219.
[6] C. Buelens, J. P. Celis and J. R. Roos, *ibid.* **13** (1983) 541.
[7] J. A. Harrison and J. Thompson, *J. Electroanal. Chem.* **40** (1972) 113.
[8] I. R. Burrows, J. A. Harrison and J. Thompson, *ibid.* **53** (1974) 283.
[9] H. Y. Cheh and R. Sard, *J. Electrochem. Soc.* **118** (1971) 1737.
[10] J. D. E. McIntyre and W. F. Peck, Jr., *ibid.* **123** (1976) 1800.
[11] D. M. MacArthur, *ibid.* **119** (1972) 672.
[12] E. T. Eisenmann, *ibid.* **125** (1978) 717.
[13] M. Beltowska-Brzezinska, E. Dutkiewicz and W. Lawicki, *J. Electroanal. Chem.* **99** (1979) 341.
[14] P. Bindra, D. Light, P. Freudenthal and D. Smith, *J. Electrochem. Soc.* **136** (1989) 3616.
[15] G. A. Kurnoskin, V. N. Flerov, A. N. Moskvichev and A. O. Rózhdestvenskii, *Élektrokhimiya* **22** (1987) 1124.
[16] A. Survila, V. Mockevicius and R. Višomirskis, *ibid.* **23** (1987) 816.
[17] J. Horkans and L. T. Romankiw, *J. Electrochem. Soc.* **124** (1977) 1499.
[18] J. W. M. Jacobs and J. M. G. Rikken, *ibid.* **136** (1989) 3633.
[19] V. J. Scocha, E. Raub and A. Knödler, *Metalloberflaeche-Angew, Electrochem.* **27** (1973) 1.
[20] B. Vincent, P. Bercot, G. F. Creusat, G. Messin and J. Pagetti, *Plat. Surf. Finish.* **77** (1990) 71.
[21] J. A. Harrison and J. Thompson, *J. Electroanal. Chem.* **59** (1975) 273.
[22] D. Davidović and R. R. Adzić, *Electrochim. Acta* **33** (1988) 103.
[23] E. Matulionis and A. Dziuve, *Chemija* **178** (1990) 44.
[24] S. T. Rao and R. Weil, *J. Electrochem. Soc.* **127** (1980) 1030.
[25] S. T. Rao and R. Weil, *Trans. Inst. Met. Finish.* **57** (1979) 97.
[26] K. Lin, R. Weil and K. Desai, *J. Electrochem. Soc.* **133** (1986) 690.
[27] K. L. Lin, W. C. Liu, M. H. M. Lin and Y. W. Liu, *ibid.* **138** (1991) 3276.
[28] G. Holmbom and B. E. Jacobson, *ibid.* **135** (1988) 2720.
[29] C. Bocking and C. Cameron, *Trans. I. M. F.* **72** (1994) 33.
[30] C. Bocking and C. Dineen, *ibid.* **72** (1994) 101.
[31] W. Chrzanowski, Y. G. Li and A. Lasia, *J. App. Electrochem.*, in press.
[32] Y. G. Li and A. Lasia, *J. Appl. Electrochem.* **26** (1996) 853–863.
[33] M. Fleischmann and H. R. Thirsk, *in* 'Advances in Electrochemistry and Electrochemical Engineering', Vol. 3 (edited by P. Delahay and C. Tobias) Wiley Interscience, New York (1963), p. 123.
[34] J. A. Harrison and H. R. Thirsk, *in* 'Electroanalytical Chemistry', Vol. 5 (edited by A. J. Bard) Marcel Dekker, London (1971), p. 67.
[35] I. R. Burrows, J. A. Harrison and J. Thompson, *J. Electroanal. Chem.* **58** (1975) 241.
[36] J. A. Harrison, H. B. Sierra Alcazar and J. Thompson, *ibid.* **53** (1974) 145.
[37] A. Hernández Creus, P. Carro, S. González, R. C. Salvarezza and A. J. Arvia, *Electrochim Acta* **37** (1992) 2215.
[38] M. Y. Abyaneh and M. Fleischmann, *J. Electroanal. Chem.* **119** (1981) 187, 197.
[39] M. Y. Abyaneh, J. Hendrikx, W. Visscher and E. Barendrecht, *J. Electrochem. Soc.* **129** (1982) 2654.
[40] V. G. Roev and N. V. Gudin, *Elektrokhimiya* **31** (1995) 532.
[41] A. J. Bard and L. R. Faulkner, 'Electrochemical Methods (Fundamentals and Applications)', John Wiley & Sons, New York (1980), p. 304.
[42] Y. G. Li and A. Lasia, under preparation.
[43] D. S. Gnanamuthu and J. V. Petrocelli, *J. Electrochem. Soc.* **114** (1967) 1036.
[44] S. Nakahara and Y. Okinaka, *ibid.* **128** (1981) 284.
[45] G. Holmbom and B. E. Jacobson, *ibid.* **135** (1988) 787.
[46] Y. Okinaka and S. Nakahara, *ibid.* **123** (1976) 1284.

[47] Y. Okinaka, Proceedings of the Symposium on Electrodeposition Technology, Theory and Practice, Electrochemical Society, Pennington NJ (1987), p. 147.
[48] G. B. Munier, *Plating* **56** (1967) 1151.
[49] H. Baltruschat and J. Heitbaum, *J. Electroanal. Chem.* **157** (1983) 319.
[50] D. H. Son and K. Kim, *Bull. Korean Chem. Soc.* **15** (1994) 357.
[51] E. B. Budevski, *in* 'Comprehensive Treatise of Electrochemistry', Vol. 7 (edited by B. E. Conway, J. O'M. Bockis, E. Yeager, S. U. M. Khan and R. E. White), Plenum Press, London (1983), p. 399 and references therein.